AD

TECHNICAL REPORT ARCCB-TR-98012

PHASE, RESIDUAL STRESS, AND TEXTURE IN TRIODE-SPUTTERED TANTALUM COATINGS ON STEEL

S. L. LEE
D. WINDOVER

JULY 1998

US ARMY ARMAMENT RESEARCH, DEVELOPMENT AND ENGINEERING CENTER
CLOSE COMBAT ARMAMENTS CENTER
BENÉT LABORATORIES
WATERVLIET, N.Y. 12189-4050

APPROVED FOR PUBLIC RELEASE; DISTRIBUTION UNLIMITED

DISCLAIMER

The findings in this report are not to be construed as an official Department of the Army position unless so designated by other authorized documents.

The use of trade name(s) and/or manufacturer(s) does not constitute an official indorsement or approval.

DESTRUCTION NOTICE

For classified documents, follow the procedures in DoD 5200.22-M, Industrial Security Manual, Section II-19 or DoD 5200.1-R, Information Security Program Regulation, Chapter IX.

For unclassified, limited documents, destroy by any method that will prevent disclosure of contents or reconstruction of the document.

For unclassified, unlimited documents, destroy when the report is no longer needed. Do not return it to the originator.

REPORT DOCUMENTATION PAGE

Form Approved
OMB No. 0704-0188

1. AGENCY USE ONLY (Leave blank)	2. REPORT DATE	3. REPORT TYPE AND DATES COVERED
	July 1998	Final

4. TITLE AND SUBTITLE

PHASE, RESIDUAL STRESS, AND TEXTURE IN TRIODE-SPUTTERED TANTALUM COATINGS ON STEEL

5. FUNDING NUMBERS

AMCMS No. 6111.01.91A1.1

6. AUTHOR(S)

S.L. Lee and D. Windover

7. PERFORMING ORGANIZATION NAME(S) AND ADDRESS(ES)

U.S. Army ARDEC
Benet Laboratories, AMSTA-AR-CCB-O
Watervliet, NY 12189-4050

8. PERFORMING ORGANIZATION REPORT NUMBER

ARCCB-TR-98012

9. SPONSORING/MONITORING AGENCY NAME(S) AND ADDRESS(ES)

U.S. Army ARDEC
Close Combat Armaments Center
Picatinny Arsenal, NJ 07806-5000

10. SPONSORING/MONITORING AGENCY REPORT NUMBER

11. SUPPLEMENTARY NOTES

Presented at the 25th International Conference on Metallurgical Coatings and Thin Films, San Diego, CA, 27 April to 1 May 1998. Published in Proceedings of the Conference and *Surface and Coatings Technology*.

12a. DISTRIBUTION/AVAILABILITY STATEMENT

Approved for public release; distribution unlimited.

12b. DISTRIBUTION CODE

13. ABSTRACT (Maximum 200 words)

This work analyzes the unoptimized, prototype triode-sputtered. 150 μm thick tantalum coatings deposited with a 2.5 μm niobium under-layer onto the bore of a large-diameter A723 steel cylinder. The coating was deposited for wear and erosion protection by Pacific Northwest National Laboratory. Our phase determination was based on x-ray diffraction analysis, wavelength dispersive x-ray fluorescence analysis, energy dispersive x-ray analysis, and hardness and electrical resistivity measurements. Both x-ray diffraction and radius-of-curvature methods were used to determine residual stresses. A locally developed high-resolution pole figure technique was used to perform texture analysis. The post-firing, debonded coating showed alpha-tantalum, preferred [110] orientation, high surface stresses, tantalum oxides, entrapped krypton sputtering gas, interstitial oxygen, and other impurities. The surface and subsurface pole figures revealed broadened poles and body-centered-cubic tantalum crystalline structure.

14. SUBJECT TERMS

Residual Stress, Texture, Tantalum, Sputtered, Phase, Niobium, X-Ray Fluorescence, X-Ray Diffraction

15. NUMBER OF PAGES

17

16. PRICE CODE

17. SECURITY CLASSIFICATION OF REPORT	18. SECURITY CLASSIFICATION OF THIS PAGE	19. SECURITY CLASSIFICATION OF ABSTRACT	20. LIMITATION OF ABSTRACT
UNCLASSIFIED	UNCLASSIFIED	UNCLASSIFIED	UL

TABLE OF CONTENTS

LIST OF ILLUSTRATIONS

ACKNOWLEDGEMENTS

Thanks are due to D.W. Matson and J. Walden for providing the supttered cylinder; D. Crayon for the fractured coating specimens; and P. Cote, P. Chen, and J. Vasilakis for the helpful discussions.

INTRODUCTION

Tantalum has important applications in electronics and x-ray optics and it acts as a diffusion barrier material for semiconductor interconnects (refs 1,2). With the increasing demands for future pressure vessels, tantalum is a potential environmentally-friendly refractory metal for the protection of bores against high temperature wear and erosion. Cox and McClanahan (ref 3) studied high rate triode-sputtered tantalum coatings deposited under 500°C on steel, and found that the process can produce adhesive and defect-free uniform coatings. Bulk tantalum, usually in the form of alpha-tantalum, has attractive properties for wear and erosion—a high melting point; good ductility and formability; and excellent corrosion resistance to many acids, salts, and gases. However, depending on the deposition conditions, alpha, beta, or both phases may be observed. Clevenger *et al.* (ref 4) reported that thin-film sputtering generally resulted in beta-tantalum, and stress relaxation occurred during the beta to alpha-tantalum phase transition. Cabral *et al.* (ref 5) reported that sputtered beta-tantalum films subjected to thermal cycling produced a -500 MPa per cycle compressive stress increase, resulting in highly stressed, fragile films. The ability to control alpha and beta-phase tantalum nucleation and growth is highly desirable for these and other applications.

Several deposition conditions significantly influence the alpha and beta-phase formation, including impurity content, surface preparation, substrate bias and temperature, and type of substrate. Face and Prober (ref 6) reported that a niobium under-layer ensured alpha-tantalum formation. Schwartz and Feit (ref 7) studied the impurity effects on nucleation, and reported that for the same sputtering conditions, tantalum phases depended on the type of substrate. Matson *et al.* (ref 8) described sputtered alpha-tantalum on cylindrical bore surfaces using a niobium under-layer. An unoptimized, prototype triode-sputtered tantalum coating was deposited onto the bore of a thick-walled A723 steel cylinder on top of a thin niobium layer at Pacific Northwest National Laboratory (ref 9). We report herein our analysis of the post-firing, debonded coating. Our analysis showed predominant alpha-phase nucleation and growth, high surface residual stresses, surface tantalum oxides, entrapped krypton sputtering gas, and interstitial oxygen. Surface and subsurface pole figure analysis revealed broadened poles with preferred [110] orientation and the structure in the body-centered-cubic (BCC) tantalum coating. Further optimization of deposition parameters to improve adhesion, residual stress, and microstructure *via* quantitative characterization is suggested.

EXPERIMENTAL PROCEDURE

The triode-sputtering apparatus and experimental procedure used to coat the bore surfaces of a cylinder at Pacific Northwest Laboratory are described in References 3, 8, and 9. The water-cooled target located at the center anode, the steel cylinder substrate acting as the cathode, and the water-cooled thermostat are coaxial. The system was pumped to 1.0-4.0 x 10^{-7} torr. The 99.98% tantalum tube from NRC, Inc., Newton, MA, was used as the sputtering target, and 99.99% krypton at 1-3 x 10^{-3} torr was used as the sputtering gas. Approximately 2.5 μm

niobium under-layer was sputtered from the precoated tantalum target onto the steel substrate; then 150 μm tantalum was sputtered on top of the niobium layer at a rate of 0.3 μm/min. When the post-firing test cylinder was sectioned into specimens for analysis, the coating separated from the steel substrate and curled into a long cylindrical shell.

X-RAY DIFFRACTION ANALYSIS

Our phase determination included x-ray diffraction analysis, wavelength dispersive x-ray fluorescence analysis, energy dispersive x-ray analysis, and electrical resistivity and hardness measurements. Alpha-tantalum has a resistivity of 15 to 60 μΩ-cm; beta-tantalum has a resistivity of 200 μΩ-cm. A resistivity measurement of the tantalum coating using a four-point probe was 20.27 μΩ-cm, indicating that the coating was alpha-tantalum. Figure 1a shows x-ray diffraction scans obtained using Cu K-alpha radiation in log scale for the front surface and the front subsurface after 14 μm thickness was removed by hand polishing. The figure also shows the standard patterns from International Center for Diffraction Data (ICDD). Surface and sub-surface coatings show all BCC-tantalum with preferred [110] orientation, Ta_2O_5, and TaO. The relative peak intensities of surface oxides to tantalum were estimated to be 6% at the surface, and 1% at the subsurface, ignoring preferred orientation effects. Figure 1b shows x-ray diffraction scans for the back surface and back subsurface after 1 μm thickness was removed by hand polishing. The patterns show niobium, alpha-tantalum, and no trace of beta-tantalum. Since BCC-tantalum has a = 0.33058 nm, which is almost identical to niobium with a = 0.33066 nm, it is difficult to differentiate tantalum and niobium by x-ray diffraction. Therefore, energy dispersive x-ray analysis and wavelength dispersive x-ray fluorescence analysis were used to complement niobium determination. On the separated substrate steel, x-ray diffraction analysis revealed iron in shiny patches, and iron, iron carbide, and tantalum oxides in darker patches.

TEXTURE IN BODY-CUBIC-CENTERED TANTALUM COATING

Crystalline texture can significantly influence material properties. Texture and the epitaxial relation between thin-film and substrate have been used as important parameters to optimize thin-film behavior. Texture analysis was performed using locally developed software on a Scintag diffractometer using Cu radiation for the front surface and front subsurface. The results were almost identical, indicating that there was no significant texture gradient at the depth of 14μm. Figures 2a and 2b illustrate the tantalum (110), (100), (211), and (321) pole figures. The (110) pole figure had a strong central pole at $\chi = 0°$ and at $\chi = 60°$. Interplaner angles calculated were [110]/[110] = 0° and 60°. The (100) pole figure showed two poles at $\chi = 45°$. The calculated angle was [110]/[100] = 45° with twofold symmetry. The (211) pole figure showed four poles at $\chi = 30°$. The calculated angles were [110]/[211] = 30°, 54.7°, and 73.2°, with fourfold symmetry expected at 30°. The (321) pole figure showed eight poles—four inner poles at $\chi = 19°$, and four outer poles at $\chi = 40°$. The calculated interplaner angles were [110]/[321] = 19°, 41°, and 55°, with fourfold symmetry expected for both 19° and 41°. The broad poles arose because of the distribution of grains with orientations slightly off axis. This work completely characterized the structure as BCC-tantalum with [110] orientation.

WAVELENGTH DISPERSIVE X-RAY FLUORESCENCE ANALYSIS

Wavelength dispersive x-ray fluorescence analysis was performed using an Rh tube and PET, LiF220, LiF200, and OVO55 crystals on a Siemens SRS3000. The front surface consisted of tantalum, oxygen, carbon, magnesium, aluminum, calcium, and silicon; the front subsurface consisted of tantalum, oxygen, magnesium, aluminum, calcium, and silicon. The back surface consisted of tantalum, niobium, oxygen, iron, and manganese; the back subsurface consisted of tantalum, niobium, oxygen, iron, and silicon. Because of the finite penetration depth of the Rh x-rays and the thin niobium layer, the back surface showed both niobium and tantalum concentrations. Figure 3 compares the relative intensities of tantalum, niobium, oxygen, and krypton peaks. The data disclosed the collowing:

- The front surface consisted of tantalum and oxygen, no niobium, and low krypton peaks.
- The front sub-surface consisted of increased tantalum, decreased oxygen peaks, no niobium, and low krypton peaks.
- The back surface consisted of niobium, reduced tantalum and oxygen, and high krypton peaks.
- The back polished surface consisted of decreased niobium and tantalum, reduced oxygen, and high krypton peaks.

The OVO55 crystal was not sensitive to nitrogen. Cote (ref 10) recently reported that a chemical analysis performed by Leco Corporation calculated approximately 1.6 weight percent of oxygen plus nitrogen total. Preliminary auger analysis confirmed the oxygen and carbon, but showed low nitrogen concentrations. Wavelength dispersive x-ray fluorescence analysis of the steel substrate showed the major components of steel, including iron, nickel, chromium, molybdenum, manganese, carbon, silicon, vanadium, phosphorus, sulfur, carbon, and oxygen, with trace tantalum and niobium concentrations.

HARDNESS AND PHOTOMICROGRAPHS

Alpha-tantalum has a hardness of 100 to 200 Knoop, while beta-tantalum has a hardness of 1000 to 1200 Knoop. Hardness of the growth surface and transverse sections was measured using diamond pyramid and Knoop indentors on a Leitz metallography tester and a Leco M400 hardness tester. A consistent deposition hardness of 350 Vickers at a 50-gram load, and 355 KHN-50 were obtained, which was close to the hardness for alpha-tantalum. The photomicrograph technique was used to reveal the differences in color and texture brought out by polishing—the harder beta-phase appears lighter, the softer alpha-phase appears darker. Figure 4 shows a photomicrograph of sputtered alpha-tantalum on iron at 500X. This can be compared to Figure 4a, which shows electrochemical tantalum deposition on copper in molten salt (see ref 11) and Figure 4b, which shows our cylindrical magnetron sputter-deposited tantalum on iron.

X-RAY RESIDUAL STRESSES

The anisotropy factor and aggregate elastic constants of tantalum have been calculated from single-crystal elastic constants assuming isotropic elastic models (ref 12). Hill and Neerfeld showed that Voigt's uniform strain model and Reuss's uniform stress model are the least upper-bound and greatest lower-bound of the elastic constants, and suggested averaging the two. We used an average E = 185.4 GPa and $\mu = 0.341$ for tantalum in our residual stress analysis. X-ray diffraction *d*-spacing versus $\sin^2 \psi$ is one of the most established methods of residual stress analysis. However, it is applicable only for isotropic or weakly textured materials. Triode-sputtered tantalum exhibited relatively weak texture, shown by comparing the normalized intensities of the reflections in the coatings to random powder. Furthermore, the calculated anisotropy factor, defined as $2C_{44}/(C_{11} - C_{12}) = 1.56$ was relatively low for tantalum.

Figure 5 illustrates the residual stress of the front coating surface using the tantalum [220] reflection at 157.81° 2θ using chromium K-alpha radiation. A good linear curve was obtained for the front coating surface, giving tantalum an 810 ±44 MPa tensile stress in the longitudinal direction, and a 511 ±99 MPa stress in the hoop direction. The larger experimental error in hoop stress measurement was due to the specimen curvature. Relaxation in the hoop direction may have resulted in lower stress in the hoop direction compared to the longitudinal direction. Surface residual stress on the back niobium side was compressive by looking at the direction of the peak shifts at various Ψ-tilts. The measurement suffered from large errors due to texture and the presence of both niobium [220] at 156.76° and tantalum [220] at 156.81° diffraction peaks, which were difficult to differentiate. The total net stress in the coating is expected to be zero. No stress depth profiling was performed, but the tensile stress on the front surface is expected to gradually change to compressive stress toward the back surface.

RESIDUAL STRESS BY RADIUS-OF-CURVATURE CALCULATION

Several researchers have used the curvature method to study residual stresses in spalled coatings (refs 13,14). From the theory of a bending plate (ref 15)

$$\rho = (E_C * I)/(M * (1 - \mu_C^2))$$

where M is the bending moment, I is moment of inertia, ρ is the measured radius-of-curvature, E_C is Young's modulus of the coating, and μ_C is Poisson's ratio of the coating. Assuming σ is the stress, and C is half thickness of the coating, stress σ can be calculated as

$$\sigma = M * C/I$$

$$\sigma = (E_C * C)/((1 - \mu_C^2) * (1/\rho - 1/\rho_0))$$

where ρ and ρ_0 are the final and initial radius-of-curvature, respectively.

In our study, the initial radius was ρ_o = 60 mm. The final circumference was measured at the two ends of the intact cylindrical detached coating, C1 = 115 mm and C2 = 128 mm, giving an average radius-of-curvature of ρ = 19.3 mm. Stress determination by the radius-of-curvature method gave 554 MPa tensile hoop stress for the top surface.

FRACTURE SURFACE

Figure 6 shows a cross section of debonded tantalum/niobium film that was tensile fractured. An energy dispersive x-ray analysis of area 1a in the figure shows niobium, tantalum, iron, and oxygen. An energy dispersive x-ray analysis of area 1b shows all tantalum. Figure 6a depicts the microstructure of area 2 close to the niobium side. It exhibits a brittle intergranular separation at and near the top, and a more ductile separation near the center. Figure 6b depicts the microstructure of area 3 close to the tantalum side, which is characterized by a very ductile dimpled fracture. The surfaces containing niobium show more brittle fracture, which may be responsible for the separation of the coating from the substrate.

DISCUSSION

The exact reason for alpha and beta-phase formation is not well-known, although impurity, substrate nature, substrate condition, and substrate bias have been considered. Westwood and Livermore (ref 16) proposed that beta-tantalum is an impurity-stabilizing phase formed to accommodate oxygen or nitrogen when their concentrations in the coating exceed their solubility limit. Collobert and Chouan (ref 17) proposed the cluster theory to explain growth of alpha-tantalum on beta-tantalum. Sato (ref 18) studied the presence of oxygen and OH on the substrate surface in beta-tantalum formation, and concluded that substrates with resistance to oxidation tend to nucleate in the alpha-phase. Because of the many good properties of alpha-tantalum compared to beta-tantalum, coatings consisting of all or mostly alpha-tantalum are preferred. Moreover, from the lattice parameter point of view, BCC-tantalum has a +15.3% lattice mismatch to substrate iron, which is more favorable compared to tetragonal-tantalum. In this work, it was demonstrated that alpha-phase nucleation and growth of tantalum can be controlled by using the niobium sublayer, regardless of the impurity contents.

Impurities can influence the phase formation, adhesion, residual stress, and strength. The firing process is the likely cause of the high Ta_2O_5, TaO, and carbon concentrations observed on the front surface. It induced hot gases in addition to imparting high tensile stress loading to the cylinder bore. The observance of oxygen peaks at the niobium surface and subsurface indicated possible interstitial oxygen in the tantalum and niobium lattices. The source of the oxygen could be the target, leakage through the Viton® O-ring, surface oxides, or H_2O from the substrate. Cabral *et al.* (ref 5) reported that sputtered beta-tantalum films subjected to thermal cycling produced a high compressive stress increase due to the increased oxygen content. By an improved reverse-sputtering cleaning process, Cote (ref 10) recently showed good adherent alpha and beta-tantalum coatings using a planar magnetron sputtering-deposition system.

Residual stresses cause cracking, buckling in coatings, and debonding of the coatings from the substrate. Residual stress may be induced by grain growth, recrystallization, chemical reactions such as oxidation, phase transformation, thermal expansion coefficient mismatch and lattice mismatch between coatings and substrate, voids, and impurities. High deposition residual stresses in tantalum coatings varying between -2×10^{10} dynes/cm^2 (-2000 MPa) and 2×10^{10} dynes/cm^2 have been reported (refs 19-21). In this work, undesirable high surface residual stresses were observed on the debonded coating. Residual stress generally depends on the processing history of the specimen. In our coating, stress resulted from the triode-sputtering process; thermal expansion mismatch between tantalum, niobium, and steel; other thermal-mechanical effects due to firing; and coating separation from the substrate. Deposition residual stresses depend on the deposition parameters, such as gas pressure. By finding the zero-crossing pressure when the deposition stresses transition from a highly compressive to a highly tensile state, deposition residual stress can be minimized.

CONCLUSIONS

- Our phase analysis showed that an all alpha-tantalum coating has been achieved by triode-sputtering a coating with a niobium under-layer.

- Entrapped krypton sputtering gas, possible interstitial oxygen, and surface oxide concentrations were observed.

- Our surface and subsurface texture study completely specified the structure of the tantalum coating on steel showing broadened poles and a BCC alpha-phase structure with preferred [110] orientation.

- Our x-ray diffraction and radius-of-curvature stress analyses showed undesirable high tensile residual stresses on the front surface of the coatings.

- Improvement in the impurity content and optimization of residual stress and microstructure deposition parameters are suggested to further improve coating behavior.

REFERENCES

1. Holloway, K., and Fryer, P.M., *Appl. Phys. Lett.*, Vol. 52, No. 17, 1990, pp. 1736-3321.

2. Catania, P., Doyle, J.P., and Cuomo, J.J., *J. Vac. Sci. Technol. A*, Vol. 10, No. 5, 1992, pp. 3318-3321.

3. Cox, J.F., and McClanahan, E.D., *Proceedings of the Tri-Service Gun Tube Wear and Erosion Symposium,* 1982, pp. 277-281.

4. Clevenger, L.A., Mutscheller, A., Harper, J.M.E., Cabral, C., Jr., and Barmak, K., *J. Appl. Phys.*, Vol. 72, No. 10, 1992, pp. 4918-4924.

5. Cabral, C., Jr., Clevenger L.A., and Schad, R.G., *J. Vac. Sci. Technol. B*, Vol. 12, No. 4, 1994, pp. 2818-2821.

6. Face, D.W., and Prober, D.E., *J. Vac. Sci. Technol. A*, Vol. 5, No. 6, 1987, pp. 3408-3411.

7. Schwartz, N., and Feit, E.D., *J. Electrochem. Society: Solid State Science and Technology*, Vol. 124, No. 1, 1977, pp. 125-130.

8. Matson, D.W., Merz, M.D., and McClanahan, E.D., *J. Vac. Sci. Technol. A*, Vol. 10, No. 4, 1992, pp. 1791-1796.

9. Matson, D.W., and Greenwell, E.M., "Technical Data Package for 120-mm Tube Sputtering Program," Pacific Northwest National Laboratory, Richland, WA, submitted to Benet Laboratories, January 1994.

10. Cote, P., Private Communication, Benet Laboratories, Watervliet, NY, 1998.

11. Thompson, J.F., and Pan, S.K., "The Electrodeposition of Beta-Tantalum from Molten Salts," U.S. Army ARDEC Technical Report ARCCB-TR-90028, Benet Laboratories, Watervliet, NY, October 1990.

12. Simms, G., and Wang, H., *Single Crystal Elastic Constants and Calculated Aggregate Properties: A Handbook*, The MIT Press, 1971.

13. Howard, S.J., Tsui, Y.C., and Clyne,T.W., *Acta Metal. Mater.*, Vol. 42, No. 8, 1994, pp. 2823-2836.

14. Jorgensen, O., Horsewell, A., Sorensen, B.F., and Leisner, P., *Acta Metal. Mater.*, Vol. 43, No. 11, 1995, pp. 3991-4000.

15. Timoshenko, S., and Woinowsky-Krieger, S., *Theory of Plates and Shells*, 2nd Edition, McGraw-Hill, NY, 1959.

16. Westwood, W.D., and Livermore, F.C., *Thin Solid Films*, Vol. 5, No. 5/6, 1970, pp. 407-420.

17. Collobert, D., and Chouan, Y., *Thin Solid Films*, Vol. 55, No. 3, 1978, pp. L15-16.

18. Sato, S., *Elsevier Sequoia*, 1982, pp. 321-329.

19. Thornton, J.A., *Ann. Rev. Mater. Sci.*, 1977, pp. 239-260.

20. Thornton J.A., and Hoffman, D.W., *J. Vac. Sci. Technol.*, Vol. 14, No. 1, 1977, pp. 164-168.

21. Windischmann, H., *Crit. Rev. in Solid State and Mater. Sci.*, Vol. 17, No. 6, 1992, pp. 547-596.

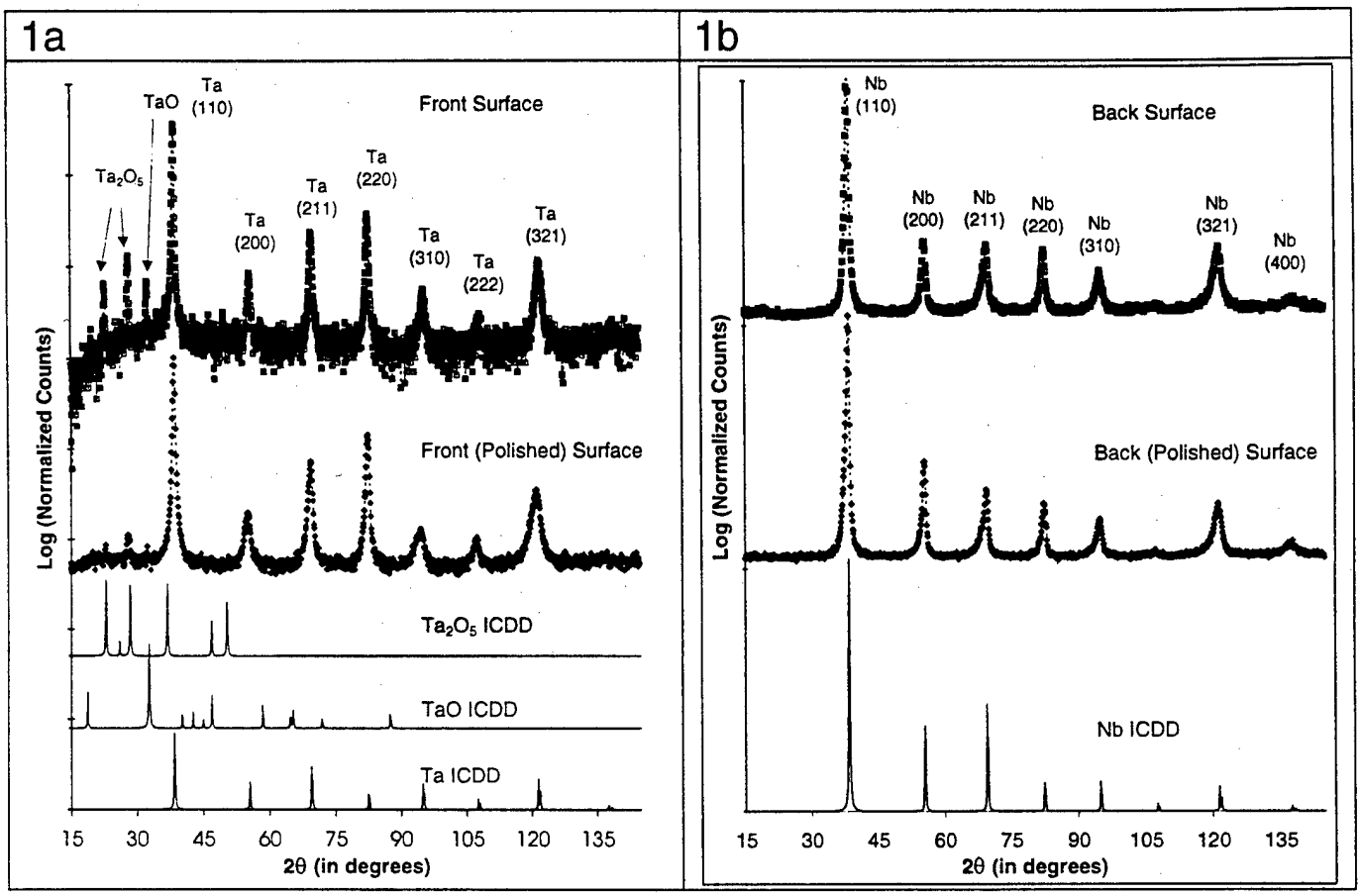

Figure 1. X-ray diffraction analysis of sputtered alpha-tantalum.

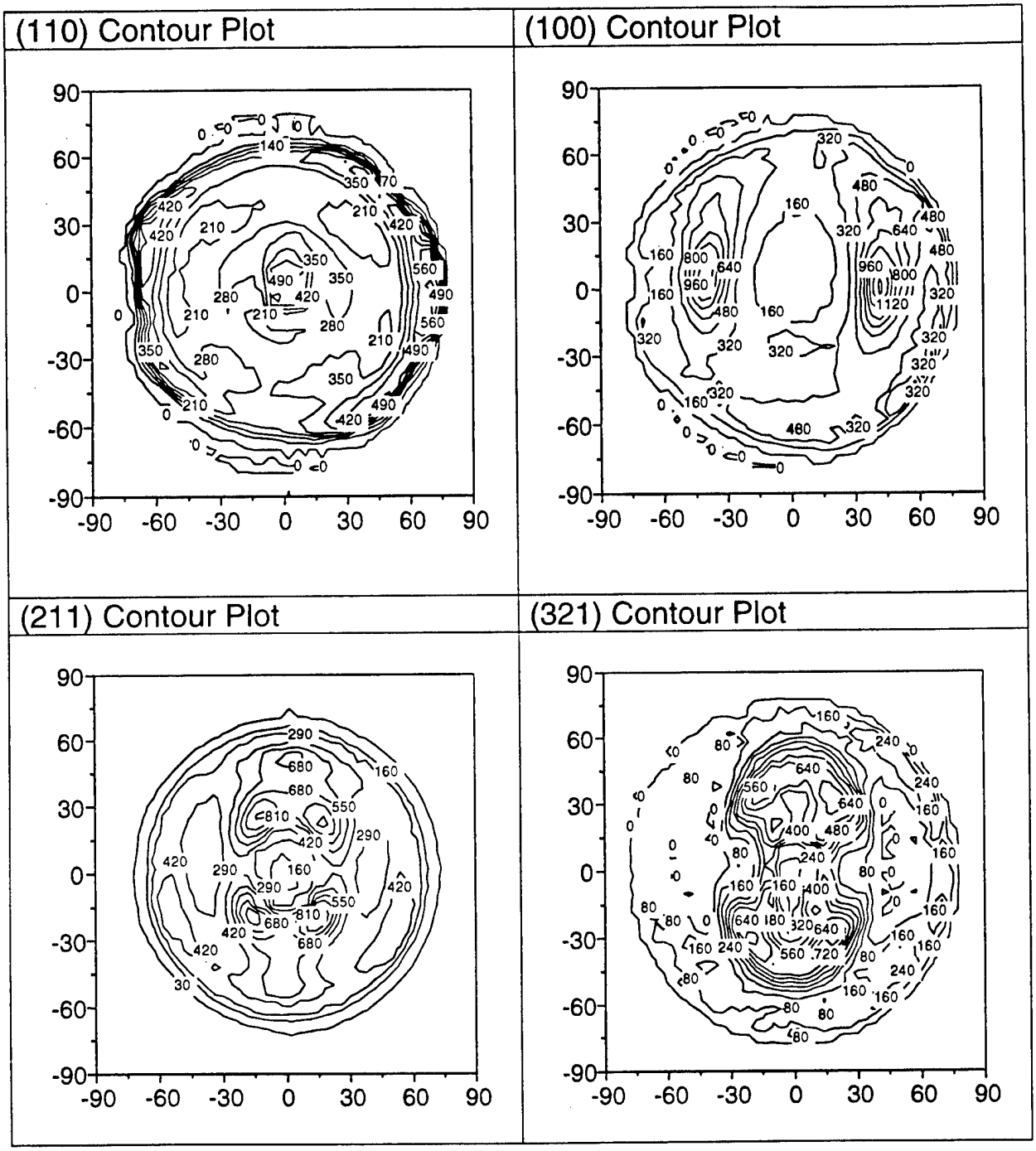

Figure 2a. Contour plots of sputtered alpha-tantalum.

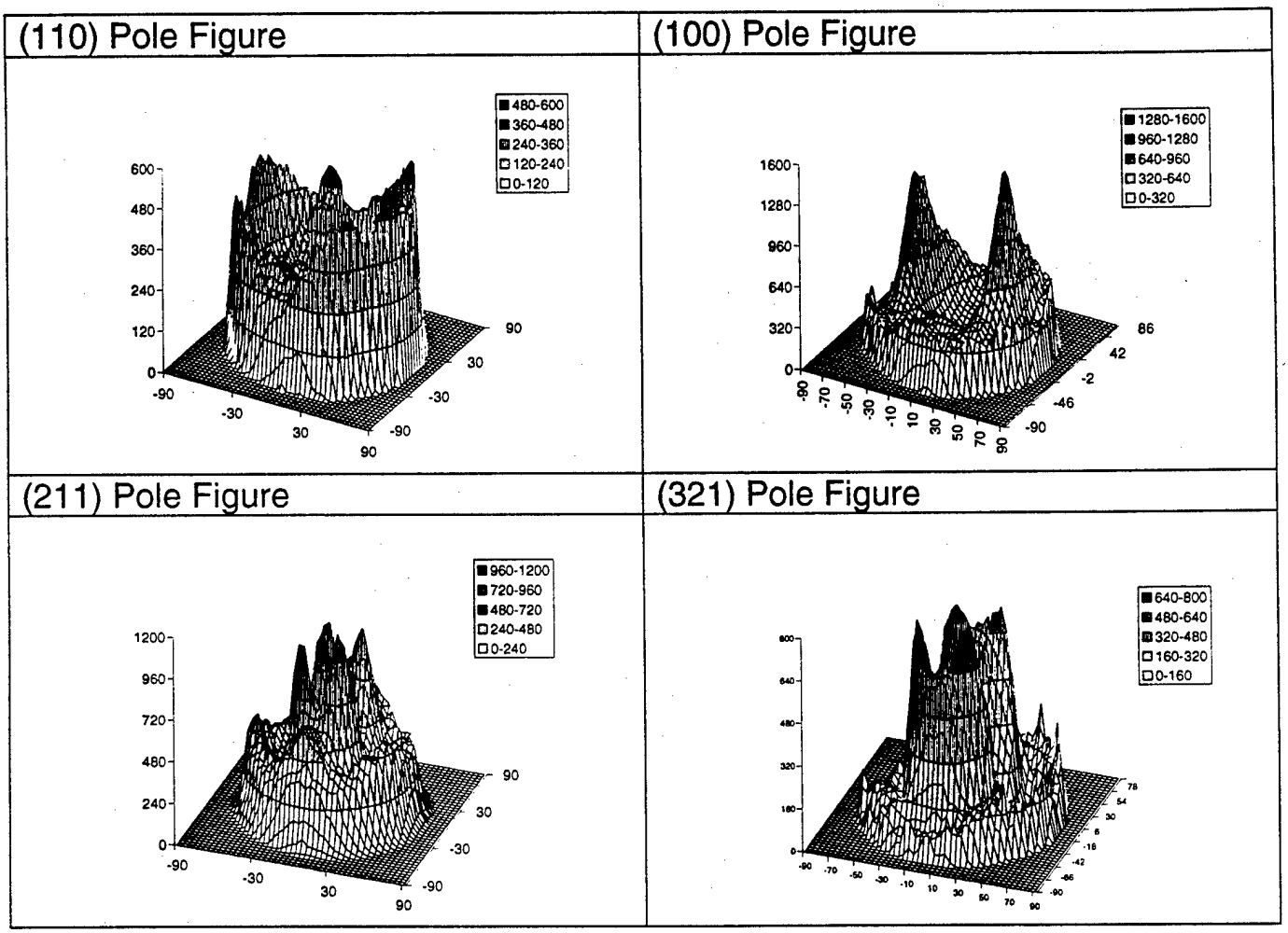

Figure 2b. Pole figures of sputtered alpha-tantalum.

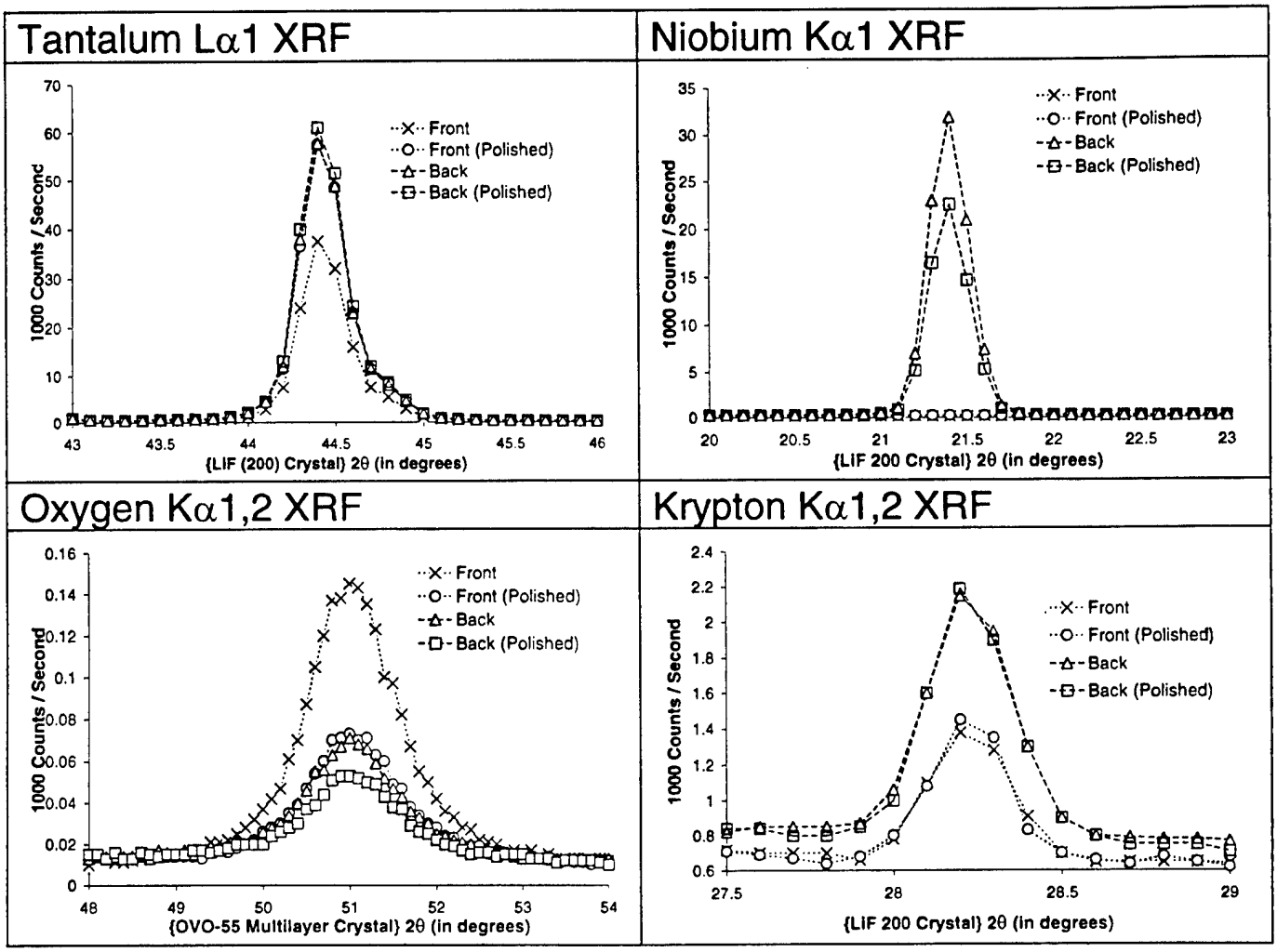

Figure 3. Wavelength dispersive x-ray fluorescence analysis of sputtered alpha-tantalum.

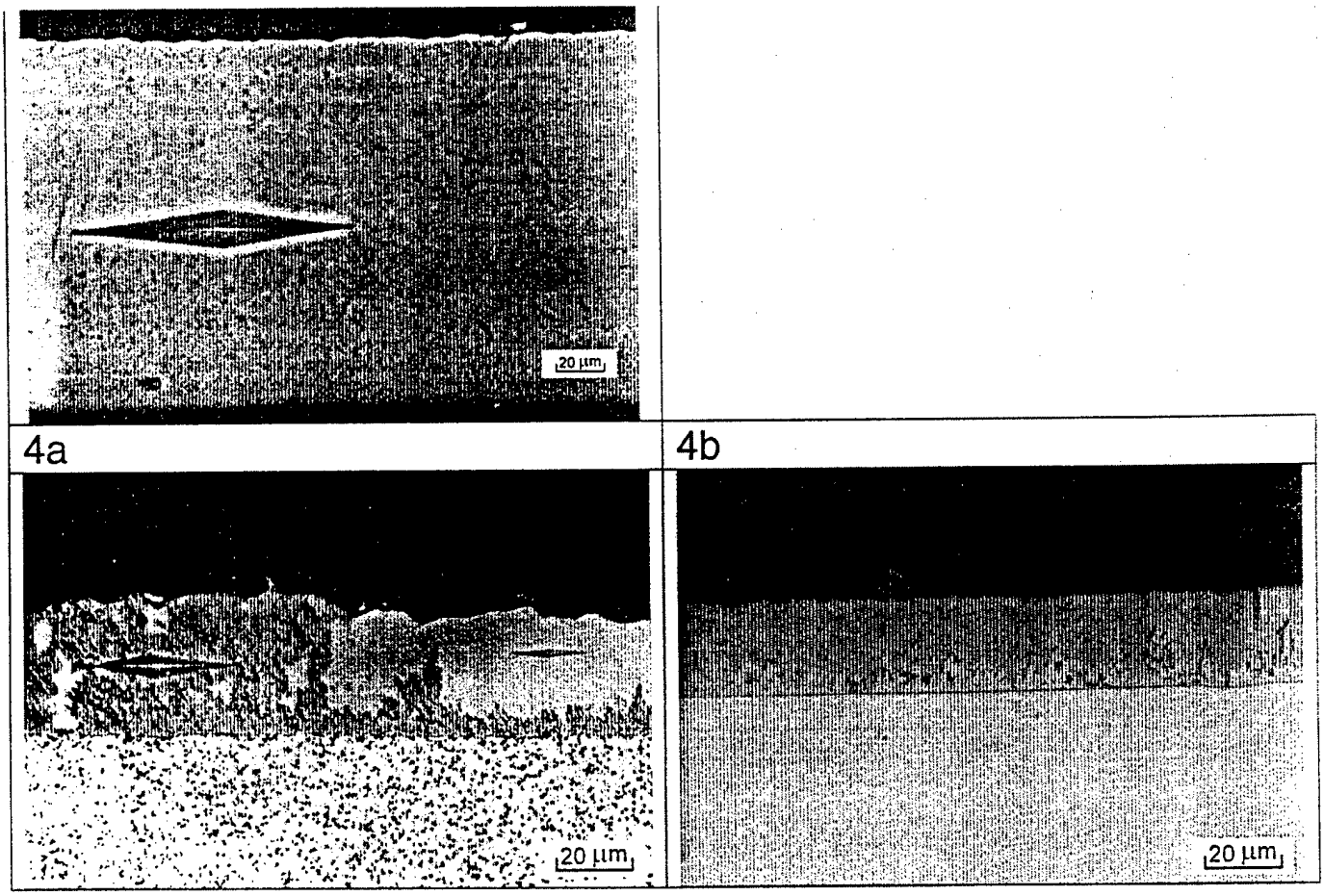

Figure 4. Photomicrographs of sputtered alpha-tantalum.

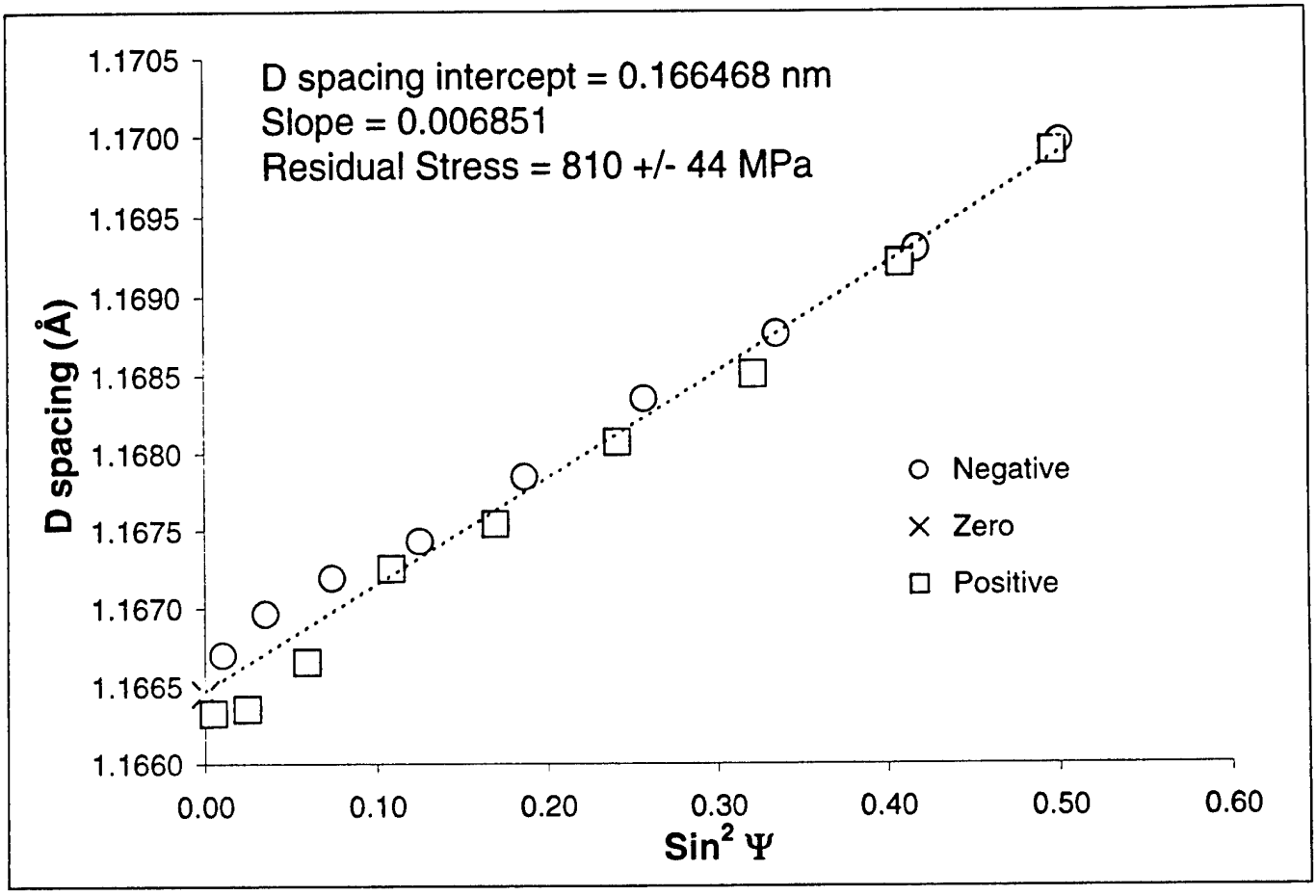

Figure 5. Residual stress in sputtered alpha-tantalum.

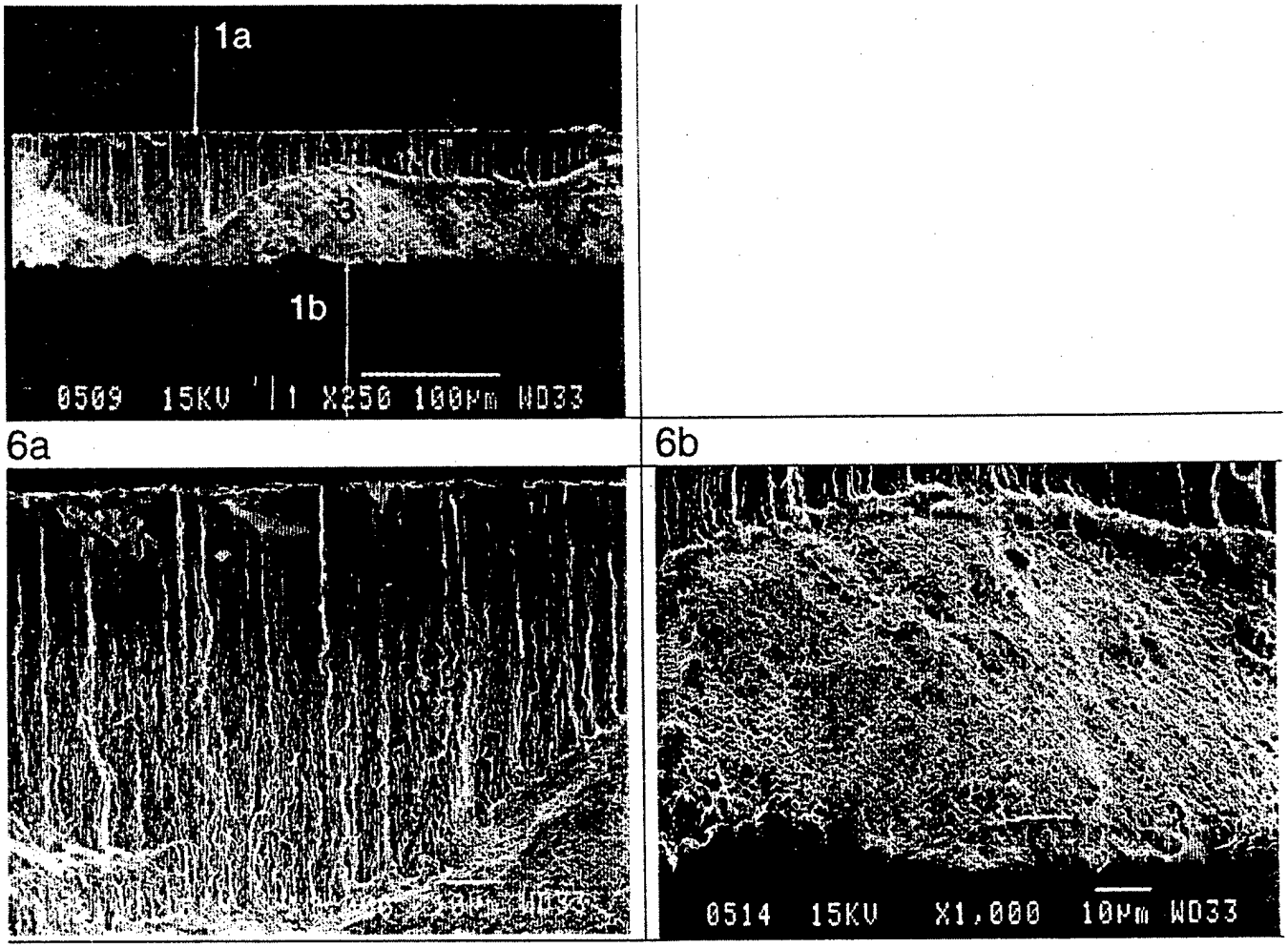

Figure 6. Fracture surface SEM of sputtered alpha-tantalum.

TECHNICAL REPORT INTERNAL DISTRIBUTION LIST

	NO. OF COPIES
CHIEF, DEVELOPMENT ENGINEERING DIVISION	
ATTN: AMSTA-AR-CCB-DA	1
-DB	1
-DC	1
-DD	1
-DE	1
CHIEF, ENGINEERING DIVISION	
ATTN: AMSTA-AR-CCB-E	1
-EA	1
-EB	1
-EC	1
CHIEF, TECHNOLOGY DIVISION	
ATTN: AMSTA-AR-CCB-T	2
-TA	1
-TB	1
-TC	1
TECHNICAL LIBRARY	
ATTN: AMSTA-AR-CCB-O	5
TECHNICAL PUBLICATIONS & EDITING SECTION	
ATTN: AMSTA-AR-CCB-O	3
OPERATIONS DIRECTORATE	
ATTN: SIOWV-ODP-P	1
DIRECTOR, PROCUREMENT & CONTRACTING DIRECTORATE	
ATTN: SIOWV-PP	1
DIRECTOR, PRODUCT ASSURANCE & TEST DIRECTORATE	
ATTN: SIOWV-QA	1

NOTE: PLEASE NOTIFY DIRECTOR, BENÉT LABORATORIES, ATTN: AMSTA-AR-CCB-O OF ADDRESS CHANGES.

TECHNICAL REPORT EXTERNAL DISTRIBUTION LIST

	NO. OF COPIES
ASST SEC OF THE ARMY RESEARCH AND DEVELOPMENT ATTN: DEPT FOR SCI AND TECH THE PENTAGON WASHINGTON, D.C. 20310-0103	1
DEFENSE TECHNICAL INFO CENTER ATTN: DTIC-OCP (ACQUISITIONS) 8725 JOHN J. KINGMAN ROAD STE 0944 FT. BELVOIR, VA 22060-6218	2
COMMANDER U.S. ARMY ARDEC ATTN: AMSTA-AR-AEE, BLDG. 3022 AMSTA-AR-AES, BLDG. 321 AMSTA-AR-AET-O, BLDG. 183 AMSTA-AR-FSA, BLDG. 354 AMSTA-AR-FSM-E AMSTA-AR-FSS-D, BLDG. 94 AMSTA-AR-IMC, BLDG. 59 PICATINNY ARSENAL, NJ 07806-5000	 1 1 1 1 1 1 2
DIRECTOR U.S. ARMY RESEARCH LABORATORY ATTN: AMSRL-DD-T, BLDG. 305 ABERDEEN PROVING GROUND, MD 21005-5066	1
DIRECTOR U.S. ARMY RESEARCH LABORATORY ATTN: AMSRL-WT-PD (DR. B. BURNS) ABERDEEN PROVING GROUND, MD 21005-5066	1
COMMANDER ROCK ISLAND ARSENAL ATTN: SMCRI-SEM ROCK ISLAND, IL 61299-5001	1
COMMANDER U.S. ARMY TANK-AUTMV R&D COMMAND ATTN: AMSTA-DDL (TECH LIBRARY) WARREN, MI 48397-5000	1
COMMANDER U.S. MILITARY ACADEMY ATTN: DEPARTMENT OF MECHANICS WEST POINT, NY 10966-1792	1
U.S. ARMY MISSILE COMMAND REDSTONE SCIENTIFIC INFO CENTER ATTN: AMSMI-RD-CS-R/DOCUMENTS BLDG. 4484 REDSTONE ARSENAL, AL 35898-5241	2
COMMANDER U.S. ARMY FOREIGN SCI & TECH CENTER ATTN: DRXST-SD 220 7TH STREET, N.E. CHARLOTTESVILLE, VA 22901	1
COMMANDER U.S. ARMY LABCOM, ISA ATTN: SLCIS-IM-TL 2800 POWER MILL ROAD ADELPHI, MD 20783-1145	1

NOTE: PLEASE NOTIFY COMMANDER, ARMAMENT RESEARCH, DEVELOPMENT, AND ENGINEERING CENTER, BENÉT LABORATORIES, CCAC, U.S. ARMY TANK-AUTOMOTIVE AND ARMAMENTS COMMAND, AMSTA-AR-CCB-O, WATERVLIET, NY 12189-4050 OF ADDRESS CHANGES.

TECHNICAL REPORT EXTERNAL DISTRIBUTION LIST (CONT'D)

	NO. OF COPIES
COMMANDER U.S. ARMY RESEARCH OFFICE ATTN: CHIEF, IPO P.O. BOX 12211 RESEARCH TRIANGLE PARK, NC 27709-2211	1
DIRECTOR U.S. NAVAL RESEARCH LABORATORY ATTN: MATERIALS SCI & TECH DIV WASHINGTON, D.C. 20375	1
WRIGHT LABORATORY ARMAMENT DIRECTORATE ATTN: WL/MNM EGLIN AFB, FL 32542-6810	1
WRIGHT LABORATORY ARMAMENT DIRECTORATE ATTN: WL/MNMF EGLIN AFB, FL 32542-6810	1

NOTE: PLEASE NOTIFY COMMANDER, ARMAMENT RESEARCH, DEVELOPMENT, AND ENGINEERING CENTER, BENÉT LABORATORIES, CCAC, U.S. ARMY TANK-AUTOMOTIVE AND ARMAMENTS COMMAND, AMSTA-AR-CCB-O, WATERVLIET, NY 12189-4050 OF ADDRESS CHANGES.